G. Manzo, M. Casu, A.C. Rinaldi, N.P. Montaldo, A. Luganini, G. Gribaudo, M.A. Scorciapino

The folded structure and insertion depth of the frog-skin antimicrobial peptide Esculentin-1b(1-18) in the presence of differently charged membrane mimicking micelles

JOURNAL OF NATURAL PRODUCTS (2014) 77
DOI: 10.1021/np5004406

The Folded Structure and Insertion Depth of the Frog-skin Antimicrobial Peptide Esculentin-1b(1-18) in the Presence of Differently Charged Membrane Mimicking Micelles

Giorgia Manzo,[†] Mariano Casu,[†] Andrea C. Rinaldi,[‡] Nicola P. Montaldo,[‡] Anna Luganini,[§] Giorgio Gribaudo,[§] Mariano A. Scorciapino[‡,]*

[†] Department of Chemical and Geological Sciences, University of Cagliari, Cittadella Universitaria, I-09042 Monserrato (CA), Italy

[‡] Department of Biomedical Sciences, University of Cagliari, Cittadella Universitaria, I-09042 Monserrato (CA), Italy

[§] Department of Life Sciences and Systems Biology, University of Torino, I-10123 Torino, Italy

* To whom correspondence should be addressed:

Tel: +39-070-675-3921.

Fax: +39-070-675- 4527.

E-mail: scorciapino@unica.it

ABSTRACT

Antimicrobial peptides (AMPs) are effectors of the innate immunity of most organisms. Their role in the defense against pathogen attack and their high selectivity for bacterial cells make them attractive for the development of a new class of antimicrobial drugs. The N-terminal fragment of the frog-skin peptide esculentin-1b (Esc(1-18)) has shown broad spectrum antimicrobial activity. Similarly to most cationic AMPs, it is supposed to act by binding to and damaging the negatively charged plasma-membrane of bacteria. Differently from many other AMPs, Esc(1-18) activity is preserved in biological fluids such as serum. In this work, a structural investigation was performed through NMR spectroscopy. The 3D structure was obtained in the presence of either zwitterionic or negatively charged micelles as membrane models for eukaryotic and prokaryotic membranes, respectively. Esc(1-18) showed a higher affinity for and deeper insertion into the latter, and adopted an amphipathic helical structure characterized by a kink at the residue G8. These findings were confirmed by measuring penetration into lipid monolayers. The presence of negatively charged lipids in the bilayer appears to be necessary for Esc(1-18) to bind, fold in the right three-dimensional structure and, ultimately, to exert its biological role as an AMP.

The lack of a new class of antibiotics is an urgent problem, as many important pathogens are rapidly developing resistance to most of the clinically usable antibiotics.[1,2] Clinical impact of antibiotic resistance is immense, with increasing length of hospital stay, costs and mortality.[3,4] Antimicrobial peptides (AMPs) have attracted the interest of the scientific community as promising candidates for the development of a new class of antimicrobial drugs. They are part of the innate immune system of the majority of the multicellular organisms, and are typically characterized by a wide spectrum of antimicrobial activity, from Gram-negative to Gram-positive bacteria, fungi, protozoa and enveloped viruses.[5–7] Despite amino acid sequence homology is not high, AMPs share some common features. They are relatively short (< 60 residues), cationic, have a large content (≥ 50%) of hydrophobic residues and adopt an amphipathic three-dimensional folding when interacting with pathogens' membranes.[6] Generally, AMPs destroy or permeate the microbial plasma-membrane. The membrane is formed through evolutionarily well conserved biosynthetic processes and represents a non-selective target, making modifications by the microorganisms difficult and, thus, resistance onset is unlikely.[8] Several recent articles have reviewed in detail the different modes of action postulated for AMPs.[9–11]

The amphipathic conformation adopted by the AMP, with the hydrophilic residues interacting with the polar head groups of the phospholipids and the water molecules, and the hydrophobic residues being protected from water contacts by inserting into the lipid bilayer core, is considered essential for it to exert the antimicrobial activity. Also the net positive charge plays a fundamental role. The content of negatively charged lipids is generally higher for microbial than eukaryotic cell membranes,[6,12,13] thus, AMPs are electrostatically attracted by the former to a greater extent, on the one hand, and cytotoxicity is kept relatively low on the other. In this scenario, the characterization of the 3D structure of AMPs when interacting with suitable membrane mimicking models is absolutely needed to deeply investigate peptide-membrane interactions at a molecular level and to provide fundamental information about the mechanism underlying the antimicrobial activity. This is

extremely important in order to improve peptide efficacy and selectivity through rational drug design.[14]

Esculentin-1b is the most active peptide (among four families) extracted from the granular glands of the skin of the frog *Rana esculenta*,[15–17] more recently classified as *Pelophylax lessonae/ridibundus*.[18] Previous studies demonstrated that its outstanding antimicrobial activity is mostly due to the N-terminal fragment comprising the first 18 amino acid residues, Esc(1-18): NH_2-GIFSKLAGKKLKNLLISG-$CONH_2$.[17,19,20] Biological investigations demonstrated broad spectrum antimicrobial activity against different fungal and bacterial species, especially Gram-negative strains, including multidrug-resistant clinical isolates, while effects on erythrocytes were negligible.[17,20,21] Remarkably, it displayed comparable activity in the presence of human serum, differently from most of the known AMPs.[20,21] More recently, an anti-*Candida* activity has also been found both *in vitro* and *in vivo* using *Caenorhabditis elegans*.[22] Esc(1-18) was found to permeate both the outer and the inner membrane of *Escherichia coli* and such a membrane perturbation was suggested as the main mechanism of action against both bacteria[21] and yeasts.[22] Possibly, membrane perturbation and increased permeability are also responsible for the reported synergism between Esc(1-18) and conventional antibiotics,[21] suggesting possible development either as an antimicrobial and/or an adjuvant drug.

Despite the availability of appreciable information describing biological activity, the active three-dimensional structure of Esc(1-18) in the lipid membrane still needs to be elucidated. The very first data on this aspect were collected with circular dichroism spectroscopy (CD), suggesting a straight α-helix encompassing the whole amino acid sequence when Esc(1-18) binds lipid vesicles.[21] In recent work from our group a more detailed structural investigation was performed with CD and NMR spectroscopy in different H_2O/trifluoroethanol (TFE) mixtures.[23] A globally amphipathic structure was found, with a helical conformation for the N-terminal portion (encompassing the first 12 residues) and an unfolded C-terminal fragment.[23] However, as the H_2O/TFE solvent is an isotropic environment, such a structural model for Esc(1-18) should be taken with caution. Despite

promoting peptide folding by favoring intramolecular H-bonds, indeed, H_2O/TFE mixtures inherently lack the intrinsic anisotropic character of a lipid bilayer.

The present work reports a more realistic structural model for Esc(1-18) obtained through liquid-state NMR investigations in the presence of suitable anisotropic membrane models. In particular, both zwitterionic and negatively charged micelles have been employed to model eukaryotic and prokaryotic plasma membrane, respectively, as bacterial membranes are usually characterized by a higher content of negatively charged lipids than the former.[6,12,13] The insertion depth of Esc(1-18) into the micelles was estimated by using Mn^{2+} ions as a paramagnetic probe. The results clearly confirm the helical folding of Esc(1-18) and show how binding and folding are prominent only in the presence of a negatively charged membrane.

RESULTS AND DISCUSSION

Sodium dodecylsulfate (SDS) and dodecylphosphocholine (DPC) are the most widely used detergents for liquid-state NMR structural determination of membrane active peptides.[24] The former is negatively charged, the latter is zwitterionic at neutral pH. AMPs are usually positively charged, while bacterial membranes are typically characterized by a higher content of anionic lipids than the eukaryotic ones, thus the electrostatics is clearly fundamental in peptide–membrane interactions. Pure DPC micelles are commonly used to mimic eukaryotic membranes, because DPC and phosphatidylcholines, the most abundant lipid class in eukaryotes, have the same head group. On the other hand, bacterial membranes are typically mimicked with pure SDS micelles, despite membranes constituted only by negatively charged phospholipids are rare. However, DPC and SDS are synergic in water and form mixed micelles of different composition, thus allowing tuning of the negative charge of this membrane model.[24]

In the present work, pure DPC and DPC/SDS mixed micelles at 3/1 molar ratio were used to mimic the plasma-membrane of an eukaryotic and a prokaryotic cell, respectively. This particular DPC/SDS molar ratio was chosen to be close to that between zwitterionic and negatively charged

lipids typical for the inner membrane of Gram-negative bacteria.[25] Table S1 reports the ^{1}H and ^{13}C resonance assignments for Esc(1-18) in the presence of either DPC or DPC/SDS micelles, obtained through a set of two-dimensional homo- and heteronuclear experiments, namely, DQF-COSY, TOCSY, NOESY, and HSQC. Figures 1a and 1b show the deviations of the observed chemical shifts from the reference 'random coil' values for $^{1}H\alpha$ and $^{13}C\alpha$, respectively. Residues present in α-helical polypeptide portions are typically characterized by a negative deviation of their $^{1}H\alpha$ chemical shift with respect to the 'random coil' value. Correspondingly, the $^{13}C\alpha$ chemical shift deviation is positive. However, only if at least four consecutive residues fit to these statistical criteria, an α-helical conformation can be hypothesized for that specific portion of the peptide under investigation.[26–28] In the presence of the purely zwitterionic micelles, only the C-terminal fragment was expected to fold in a helical conformation, because the residue S4, having the $^{13}C\alpha$ deviation from the 'random coil' chemical shift not compatible with an α-helical conformation (Figure 1b), interrupts the above mentioned series of four residues (at least) for the N-terminal fragment. On the other hand, in the presence of the negatively charged micelles, Esc(1-18) was expected to fold in an α-helical conformation from the N-terminus to the C-terminus with the regular secondary structure probably interrupted in the middle of the sequence. A more accurate secondary structure prediction was performed through the application of the software TALOS+,[29] which compares the experimental chemical shift values with a database of proteins of known 3D structure. Figures 1c and 1d show the predicted Φ/Ψ backbone angles on the Ramachandran plot together with the estimated uncertainty. In the presence of either DPC or DPC/SDS micelles, with the exception of the very first and last residues, all of the backbone angles were predicted to be very close to the α-helix region of the Ramachandran plot. In both cases, the software predictions for the almost central residue G8 had a low consensus (and were not included in Figure 1), suggesting a flexible kink that divides the peptide sequence into two helical fragments. However, in the case of pure DPC micelles, the residue S4, which is exactly in the middle of the N-terminal fragment, was predicted to

have Φ/Ψ values not compatible with an α-helix (Figure 1c), thus suggesting a regular secondary structure only for the C-terminal fragment.

Figure 2 summarizes the sequential NOEs unambiguously identified for Esc(1-18) in the presence of either DPC or DPC/SDS micelles. Figure S1 show the Hα-HN region of the NOESY spectra. A significant difference emerged between the two models, in good agreement with the TALOS+ predictions. In the presence of the purely zwitterionic DPC micelles, relatively few NOEs were found (Figure 2a). The majority were identified as Hα-HN dipolar interactions between residues located at a distance of up to four positions along the amino acid sequence. This specific pattern of sequential NOEs is typically observed for peptides folded in a helical conformation,[30] but in the case of DPC micelles these were found, basically, only in the C-terminal part of Esc(1-18). On the other hand, in the presence of negatively charged DPC/SDS micelles, the number of sequential NOEs was significantly higher (Figure 2b). The coherent series of sequential NOEs identified for different classes of protons, clearly bolstered the aforementioned predictions, and Esc(1-18) appeared to have folded in a helix-kink-helix secondary structure. The NOEs pattern, indeed, is interrupted at the level of the residue G8, strongly suggesting the presence of a flexible kink. A total of four Hα-HN(i,i+5) NOEs were also identified.

A simulated annealing protocol was applied for both cases through the software Dynamo (http://spin.niddk.nih.gov/NMRPipe/dynamo/). Only unambiguously assigned NOEs were used to set up interproton distance restraints, and only TALOS+ predictions with a high consensus score were used to set up backbone torsion angle restraints. As expected, in the case of pure DPC micelles, a helical conformation was obtained only for the C-terminal fragment. On the other hand, in the case of mixed micelles, the structure calculations confirmed all of the aforementioned observations, resulting in a structure characterized by two helical fragments (although not perfectly regular like a canonical α-helix) separated by a kink at residue G8. Table 1 summarizes the number of NMR-derived restraints and structure quality statistics for both cases. Distance restraint violations were negligible and only slight violations from the backbone dihedral restraints were

observed, with the maximum value for residues adjacent to G8 in both cases. In particular, the backbone root mean square deviation (RMSD) analysis performed for the 100 conformers with the lowest potential energy (out of the 1000 computed) showed that the peptide conformation was very well defined in the presence of the mixed micelles, while only poor resolution was achieved in the presence of the purely zwitterionic ones. However, the significantly high value of RMSD obtained in the latter case was mostly due to the N-terminal fragment. The RMSD computed only for the helical C-terminal segment was significantly lower than that obtained for the whole amino acid sequence (Table 1), although still remarkably higher than that obtained in the presence of the mixed micelles.

In the case of DPC micelles, which have no net charge at neutral pH, the electrostatic contribution to the peptide/micelle binding is probably negligible and the poor structure resolution might be due to rather weak binding interactions. Figure S2 shows the 100 conformers with the lowest potential energy after alignment of the C-terminal helix.

On the other hand, in the presence of the DPC/SDS mixed micelles, the whole peptide sequence alignment resulted in a remarkably narrow backbone RMSD distribution, with 93 conformers (out of 100) having a value less than 0.05 nm from the average structure. Compared to the purely zwitterionic DPC micelles, the well defined conformation for Esc(1-18) in the presence of the negatively charged DPC/SDS micelles clearly indicates a stronger interaction with the latter, favoring the folding. This is in line with the cationic nature of the peptide and the net negative charge of the membrane model, showing the importance of electrostatic attraction both for peptide binding and folding. Figure 3a shows a 3D representation of the backbone of Esc(1-18) in the presence of the DPC/SDS 3/1 mol/mol micelles for the 100 conformers with the lowest potential energy, according to the Dynamo force-field and the experimental NMR restraints. The overall conformation of the peptide consisted of two helical segments on either side of a kink at residue G8. This feature seems to be fundamental to have a global amphipathic structure, which would not be the case for a straight canonical α-helix encompassing the entire peptide sequence.[21,23] Both helical

fragments obtained from the present NMR investigation are actually amphipathic (Figures 3b, 3c), and the presence of a glycine residue between the two endows Esc(1-18) with sufficient plasticity to adopt a helix-kink-helix conformation, compatible with an amphipathic peptide bound to a lipid bilayer, with the hydrophobic residues being protected from water contacts by inserting into the lipid bilayer core, and the hydrophilic residues interacting with the polar head groups of the phospholipids and the waters of hydration.

Additional NMR experiments were carried out with Mn^{2+} as a paramagnetic probe. The paramagnetic ions causes a strong enhancement of both the longitudinal and the transversal relaxation rate of the water exposed nuclei. A significant intensity loss results for the corresponding cross-peaks in a 2D NMR spectrum. Such paramagnetic relaxation enhancement provides information about peptide insertion into, and orientation with respect to, the micelle surface. Being distance (and concentration) dependent, it allows discrimination of the solvent exposed residues from the micelle protected ones.[31–33] NOESY spectra were collected in the presence of Mn^{2+}, in the case of either DPC and DPC/SDS micelles, and the intensity loss of the inter-residue Hα-HN cross-peaks was monitored with respect to the intensity of the same resonances recorded in the absence of Mn^{2+} ions under the same experimental conditions. Figure 4 shows the results, with the y-axis intentionally inverted in order to have the more solvent exposed residues at the top. In the presence of DPC micelles, a marked reduction of the NOESY cross-peak intensity was observed for all the residues. Conversely, in the case of mixed DPC/SDS micelles, no significant intensity loss was observed. These results clearly indicate a dramatic difference in the behavior of Esc(1-18) depending on the charge of the membrane model employed. In agreement with what was inferred from the NMR structural analysis, cationic Esc(1-18) showed a strong binding interaction with the negatively charged DPC/SDS micelles, while the results indicated that the peptide was only weakly bound to the purely zwitterionic DPC micelle, being almost entirely exposed to the aqueous solvent in this case. These observation complement the structural analysis and bolster the primary role played by the electrostatics in determining Esc(1-18) selectivity for prokaryotic membranes, thus

the low cytotoxicity (i.e., hemolytic activity) displayed by this peptide.[17,20] Similarly to other helical AMPs,[34–37] peptide binding and insertion into the negatively charged lipid membrane is probably the first step of the mechanism of antimicrobial action.

It is also interesting to note that, for a helical peptide located right at the micelle/water interface, a markedly oscillating pattern should be expected for the residual cross-peak intensity along the amino acid sequence, with values of residual intensity ranging from ~25% to ~80% observed within a helical turn, because residues should be almost periodically exposed to or protected from the aqueous solvent where the Mn^{2+} ions are dissolved. This pattern has been actually observed, for instance, in the case of plasticin-L1, another host defense peptide recently studied by some of the authors.[33] However, the results presented here for Esc(1-18) in the presence of the DPC/SDS mixed micelles do follow a different trend, suggesting that the peptide was not merely bound on the micelle surface but more deeply buried within the detergent headgroups. Differently from Esc(1-18), plasticin-L1 does not contain positively charged residues.

Despite the results from paramagnetic relaxation enhancement experiments, only a qualitative picture of peptide localization with respect to the membrane model / water interface can be surmised. It is very interesting to note that positively charged residues are not distributed all along the Esc(1-18) sequence but rather 'concentrated' between positions 5 and 12. An additional positive charge is borne by the free N-terminus at neutral pH. Thus, it can be tentatively speculated that positive charges not only favor the peptide binding and folding, but also facilitate deeper insertion between the detergent head groups.

In the literature, it is widely reported that AMPs initially bind on top of the lipid bilayer and that their membrane insertion (and eventual pore formation) occurs only above a specific local concentration threshold.[38,39] For the sake of completeness, it should be noted that in the present investigation, i) we did not use lipid bilayers but detergent micelles, whose higher curvature and reduced size might likely alter the insertion propensity of the peptide, and ii) the peptide/detergent molar ratio of 1/100 was rather low, if compared to the expected detergent aggregation number in

the 50-70 range.[24] Most likely, our samples were characterized by only one peptide per micelle, thus the presented results can be more safely assumed to pertain to the monomeric state of Esc(1-18). Further studies with more sophisticated membrane models, such as lipid bicelles and/or solid-state NMR investigations with the use of macroscopically aligned lipid bilayers,[9] are needed to assess Esc(1-18) insertion and oligomerization propensity. In addition, it has to be emphasized that before reaching their putative target, the bacterial plasma membrane, AMPs have to cross the bacterial cell wall, which is extremely different in Gram-negative and Gram-positive bacteria, where the outermost 'layer' mainly consists of lipopolysaccharides (LPS) and peptidoglycan, respectively.[10] In the literature, examples of structural investigations of AMPs interacting with these fundamental components of the bacterial cell wall are scarce, despite being extremely interesting. It was shown, for instance, that in the presence of LPS the peptide 3D structure can be significantly different when compared to that obtained using plasma membrane models.[40–42]

Nevertheless, the results presented in this work support the idea that the presence of negatively charged lipids in the bilayer is necessary for Esc(1-18) to bind, and fold into a highly ordered three-dimensional structure. Our findings also provide an explanation for Esc(1-18) selectivity for the negatively charged plasma membranes of bacteria. The electrostatically driven binding step is the major factor in determining good selectivity, thus maintaining minimal toxicity against host cells. The structure found is consistent with the mechanism proposed for the activity of Esc(1-18).[21,22] In particular, Esc(1-18) was not found to cause the disintegration of bacteria or to form blebs on their surface but, rather, to cause the loss of cellular material through peptide-induced membrane breakages.[21] Instead of the 'classic' pore-forming activity, the peptide was supposed to bind the membrane surface in a carpet-like arrangement and insert deeply between the phospholipid head groups, with the resulting unfavorable tension generated in the bilayer ensuing in the formation of transient breakages with a size larger than 5.8 nm.[21,22] In addition, it is very interesting to note that the presence of a kink or bend in the helical folding, usually observed to occur at the position of a glycine or proline along the amino acid sequence, is a feature common to many amphipathic helical

AMPs, like cecropin A, magainin 2, caerin 1.1 and maculatin 1.1, and its importance in favoring the interaction of the peptide with the lipid bilayer has been highlighted.[14,43] It was postulated that a more rigid helix would not allow the peptide to adapt to various bacterial membranes with different composition and topology. Our current observations on the Esc(1-18) structural and mechanistic features support and further expand this model.

In recent years, monomolecular lipid layers have been increasingly used as suitable models to investigate the interaction between peptides and biological membranes.[35,44,45] We therefore used POPC and POPG monolayers to mimic a bacterial plasma membrane and to evaluate the role of electrostatics in driving peptide-membrane interactions. The surface activity of the peptide, recorded in the absence of lipids, is shown in Figure 5a. Esc(1-18) was found to be significantly active, with buffer surface pressure increasing rapidly as a function of peptide concentration. Surface pressure reached a maximum of 13.3 mN/m at a peptide concentration of 0.5 μM and remained constant at higher concentration values (up to 2.5 μM). Esc(1-18) willingly penetrated into both POPC and POPG monolayers, as shown by the surface pressure increase (Figure 5b), but it is significant that the intercalation activity was stronger in the case of negatively charged POPG films with respect to neutral POPC monolayers, at any initial surface pressure (π_0) value tested. Moreover, the kinetics of the insertion of the peptide into either POPC or POPG lipid monolayers were also analyzed and found to be significantly faster in the case of anionic films (Figure 5c, d). In general, a rapid initial peptide intercalation, upon peptide injection into the subphase, was followed by a rather stable value of π, This general kinetics pattern was apparently independent from the initial surface pressure. The very rapid intercalation resemble those found for other frog skin AMPs, temporins[35] and bombinins H,[45] and fit well with the strong surface activity of Esc(1-18), as discussed above. Taken together, these observations confirm the results obtained by NMR; a stronger interaction of Esc(1-18) with, and deeper insertion into, negatively charged micelles.

Finally, to further extend current knowledge on the biological activity of Esc(1-18), we investigated its effects on the infectivity of the membrane-enveloped Herpes simplex virus type 1 (HSV-1).

However, despite its membrane perturbing effects, Esc(1-18) did not affect HSV-1 infectivity (see Supporting Information), thus indicating that it seems to be devoid of an anti-herpesvirus activity as has been reported for esculentin-2P (Esc-2P) isolated from Rana pipiens.[46,47]

EXPERIMENTAL SECTION

General Experimental Procedures. Synthetic Esc(1-18) was purchased from ANASPEC with a purity of 95%. Perdeuterated SDS-d_{25} and DPC-d_{38}, as well as 3-(trimethylsilyl)-2,2′,3,3′-tetradeuteropropionic acid (TSP-d_4), were purchased from Cambridge Isotope Laboratories with a purity of 98%. All the other chemicals were supplied by Sigma-Aldrich.

NMR spectra were acquired with a Unity Inova 500NB high-resolution spectrometer (Agilent Technologies) operating at a ^{1}H frequency of 500.325 MHz, equipped with a high-field indirect detection probe. Experiments were carried out at 300 K, in two different buffered (phosphate buffer 10 mM, pH 7.4) micellar systems: pure DPC micelles and 3:1 mol/mol DPC/SDS micelles. In a recent study, DPC and SDS were shown to be synergistic in the formation of mixed micelles, validating their usage.[24] Lyophilized Esc(1-18) was dissolved in 700 μL of the micelle dispersion at a final concentration of 4 mM and at a peptide/detergent molar ratio of 1:100. The chemical shift scale of both ^{1}H and ^{13}C was referenced to the methyl signal of TSP (2 mM internal reference). ^{1}H spectra were acquired with a 6.7 μs pulse (90°), 1.0 s delay time, 1.0 s acquisition time and a spectral width of 6 kHz. The WET sequence was applied to suppress the H_2O signal (uburp shape was centered at the H_2O resonance with a width of 100 Hz).[48,49] DQF-COSY experiments were recorded over the same spectral window using 2048 complex points and sampling each of the 512 increments with 64 scans. The same acquisition parameters were applied for the acquisition of TOCSY spectra (MLEV-17 spin-lock scheme; 80 ms mixing time). The NOESY spectra were recorded with the same acquisition parameters and a mixing time of either 50 or 100 ms. The HSQC spectra were collected using a spectral window of 6 and 35 kHz for ^{1}H and ^{13}C, respectively.

Additional NOESY spectra were acquired under the same experimental conditions (mixing time 100 ms) after the addition of $MnCl_2$ at a final concentration of either 0.1 and 0.2 mM.

The 3D structure of Esc(1-18), either in the presence of DPC or DPC/SDS micelles, was determined using a simulated annealing protocol through the Dynamo software (http://spin.niddk.nih.gov/NMRPipe/dynamo/). Interproton distance restraints were set up by using only the unambiguous NOEs. Dipolar interactions have been classified as strong, medium, or weak on the basis of the relative intensity of the corresponding cross-peaks in the NOESY spectra, and upper limits of 0.27, 0.33, or 0.50 nm, respectively, have been applied to restrain the corresponding interproton distance. The contribution to the total potential energy was zero below the upper limit, while a harmonic potential was applied above. In addition, the software TALOS+[29] was used to analyze the chemical shift values of $^{1}H^{\alpha}$, $^{1}H^{\beta}$, $^{13}C^{\alpha}$, and $^{13}C^{\beta}$ in comparison to its high-resolution structural database, to obtain the ϕ and ψ backbone angles restraints. Only the predictions ranked as "good" were used. One thousand structures were calculated, and the 100 conformers with the lowest potential energy were selected for the analysis. Neither detergents nor H_2O molecules were present during the calculations. The selected 100 conformers were aligned, and the root-mean-square deviation (RMSD) of the backbone heavy atoms was calculated with respect to the average structure.

Insertion of Esc(1-18) into monolayers formed by either POPC or POPG was evaluated to probe the ability of the peptide to bind and penetrate microbial targets' plasma membranes. The lipids were solubilized in $CHCl_3$ and spread at an air/buffer (50 mM potassium phosphate, pH 7, with 0.1 mM EDTA) interface. Penetration was monitored by measuring surface pressure (π) with a Wilhelmy wire attached to a microbalance (DeltaPi, Kibron) and using circular glass wells (subphase volume 0.5 mL). After evaporation of the organic solvent and stabilization of monolayers at different initial surface pressures (π_0), the peptide (1 μM, final concentration) was injected into the subphase, and the increment in surface pressure of the lipid film upon intercalation of the peptide was followed for the next 35 min. The difference between the initial surface pressure and the value observed after the

penetration of Esc(1-18) into the film was taken as $\Delta\pi$. Surface activity of Esc(1-18) at the air/buffer interface was also evaluated in the absence of lipids, by injecting increasing amounts of the peptide into the subphase and measuring the variation of π with time. All measurements were performed at room temperature.

ACKNOWLEDGEMENTS

Regione Autonoma della Sardegna (P.O.R. FSE 2007−2013) is acknowledged for the Ph.D. fellowship of G. Manzo.

SUPPORTING INFORMATION AVAILABLE

Table S1 with ^{1}H and ^{13}C resonance assignments. Figures S1-S3. Experimental procedures for antiviral assays and a discussion of the results. This material is available free of charge via the Internet at http://pubs.acs.org.

REFERENCES

(1) Opar, A. *Nat. Rev. Drug Discov.* **2007**, *6*, 943–944.

(2) Tew, G. N.; Scott, R. W.; Klein, M. L.; Degrado, W. F. *Acc. Chem. Res.* **2010**, *43*, 30–39.

(3) *Antimicrobial resistance. Global report on surveillance.*; World Health Organization: Geneva, 2014.

(4) Laxminarayan, R.; Duse, A.; Wattal, C.; Zaidi, A. K. M.; Wertheim, H. F. L.; Sumpradit, N.; Vlieghe, E.; Hara, G. L.; Gould, I. M.; Goossens, H.; Greko, C.; So, A. D.; Bigdeli, M.; Tomson, G.; Woodhouse, W.; Ombaka, E.; Peralta, A. Q.; Qamar, F. N.; Mir, F.; Kariuki, S.; Bhutta, Z. a; Coates, A.; Bergstrom, R.; Wright, G. D.; Brown, E. D.; Cars, O. *Lancet Infect. Dis.* **2013**, *13*, 1057–1098.

(5) Hancock, R. E. W.; Rozek, A. *FEMS Microbiol. Lett.* **2002**, *206*, 143–149.

(6) Zasloff, M. *Nature* **2002**, *415*, 389–395.

(7) Giuliani, A.; Pirri, G.; Bozzi, A.; Di Giulio, A.; Aschi, M.; Rinaldi, A. C. *Cell. Mol. life Sci.* **2008**, *65*, 2450–2460.

(8) Peschel, A.; Sahl, H. G. *Nat. Rev. Microbiol.* **2006**, *4*, 529–536.

(9) Strandberg, E.; Ulrich, A. S. *Concepts Magn. Reson. Part A* **2004**, *23A*, 89–120.

(10) Jenssen, H.; Hamill, P.; Hancock, R. E. W. *Clin. Microbiol. Rev.* **2006**, *19*, 491–511.

(11) Nguyen, L. T.; Haney, E. F.; Vogel, H. J. *Trends Biotechnol.* **2011**, *29*, 464–472.

(12) Diamond, G.; Beckloff, N.; Weinberg, A.; Kisich, K. O. *Curr. Pharm. Des.* **2009**, *15*, 2377–2392.

(13) Epand, R. M.; Epand, R. F. *J. Pept. Sci.* **2011**, *17*, 298–305.

(14) Haney, E. F.; Hunter, H. N.; Matsuzaki, K.; Vogel, H. J. *Biochim. Biophys. Acta* **2009**, *1788*, 1639–1655.

(15) Simmaco, M.; Mignogna, G.; Barra, D.; Bossa, F. *FEBS Lett.* **1993**, *324*, 159–161.

(16) Ponti, D.; Mignogna, G.; Mangoni, M. L.; De Biase, D.; Simmaco, M.; Barra, D. *Eur. J. Biochem.* **1999**, *263*, 921–927.

(17) Mangoni, M. L.; Fiocco, D.; Mignogna, G.; Barra, D.; Simmaco, M. *Peptides* **2003**, *24*, 1771–1777.

(18) Conlon, M. J.; Kolodziejek, J.; Nowotny, N. *Biochim. Biophys. Acta - Proteins Proteomics* **2004**, *1696*, 1–14.

(19) Simmaco, M.; Mignogna, G.; Barra, D.; Bossa, F. *J. Biol. Chem.* **1994**, *269*, 11956–11961.

(20) Mangoni, M. L.; Maisetta, G.; Di Luca, M.; Marcellini, L.; Esin, S.; Florio, W.; Brancatisano, F. L.; Barra, D.; Campa, M.; Batoni, G. *Antimicrob. Agents Chemother.* **2008**, *52*, 85–91.

(21) Marcellini, L.; Borro, M.; Gentile, G.; Rinaldi, A. C.; Stella, L.; Aimola, P.; Barra, D.; Mangoni, M. L. *FEBS J.* **2009**, *276*, 5647–5664.

(22) Luca, V.; Olivi, M.; Di Grazia, A.; Palleschi, C.; Uccelletti, D.; Mangoni, M. L. *Cell. Mol. Life Sci.* **2013**.

(23) Manzo, G.; Sanna, R.; Casu, M.; Mignogna, G.; Mangoni, M. L.; Rinaldi, A. C.; Scorciapino, M. A. *Biopolymers* **2012**, *97*, 873–881.

(24) Manzo, G.; Carboni, M.; Rinaldi, A. C.; Casu, M.; Scorciapino, M. A. *Magn. Reson. Chem.* **2013**, *51*, 176–183.

(25) Epand, R. M.; Epand, R. F. *Mol. Biosyst.* **2009**, *5*, 580–587.

(26) Wishart, D. S.; Sykes, B. D.; Richards, F. M. *J. Mol. Biol.* **1991**, *222*, 311–333.

(27) Wishart, D. S.; Sykes, B. D.; Richards, F. M. *Biochemistry* **1992**, *31*, 1647–1651.

(28) Wishart, D. S.; Sykes, B. D. *J. Biomol. NMR* **1994**, *4*, 171–180.

(29) Shen, Y.; Delaglio, F.; Cornilescu, G.; Bax, A. *J. Biomol. NMR* **2009**, *44*, 213–223.

(30) Cavanagh, J.; Fairbrother, W. J.; Palmer III, A. G.; Rance, M.; Skelton, N. J. *Protein NMR Spectroscopy - Principles and Practice*; 2nd ed.; Elsevier Academic Press: Oxford, U.K., 2007.

(31) Shenkarev, Z. O.; Nadezhdin, K. D.; Sobol, V. A.; Sobol, A. G.; Skjeldal, L.; Arseniev, A. S. *FEBS J.* **2006**, *273*, 2658–2672.

(32) Abbassi, F.; Galanth, C.; Amiche, M.; Saito, K.; Piesse, C.; Zargarian, L.; Hani, K.; Nicolas, P.; Lequin, O.; Ladram, A. *Biochemistry* **2008**, *47*, 10513–10525.

(33) Scorciapino, M. A.; Manzo, G.; Rinaldi, A. C.; Sanna, R.; Casu, M.; Pantic, J. M.; Lukic, M. L.; Conlon, J. M. *Biochemistry* **2013**, *52*, 7231–7241.

(34) Wieprecht, T.; Apostolov, O.; Beyermann, M.; Seelig, J. *Biochemistry* **2000**, *39*, 442–452.

(35) Zhao, H.; Rinaldi, A. C.; Di Giulio, A.; Simmaco, M.; Kinnunen, P. K. J. *Biochemistry* **2002**, *41*, 4425–4436.

(36) Sato, H.; Feix, J. B. *Biochim. Biophys. Acta* **2006**, *1758*, 1245–1256.

(37) Mangoni, M. L. *Cell. Mol. Life Sci.* **2006**, *63*, 1060–1069.

(38) Shai, Y. *Biochim. Biophys. Acta* **1999**, *1462*, 55–70.

(39) Lee, M.-T.; Hung, W.-C.; Chen, F.-Y.; Huang, H. W. *Biophys. J.* **2005**, *89*, 4006–4016.

(40) Bhunia, A.; Saravanan, R.; Mohanram, H.; Mangoni, M. L.; Bhattacharjya, S. *J. Biol. Chem.* **2011**, *286*, 24394–24406.

(41) Bhunia, A.; Domadia, P. N.; Torres, J.; Hallock, K. J.; Ramamoorthy, A.; Bhattacharjya, S. *J. Biol. Chem.* **2010**, *285*, 3883–3895.

(42) Bhunia, A.; Ramamoorthy, A.; Bhattacharjya, S. *Chem. a Eur. J.* **2009**, *15*, 2036–2040.

(43) Hwang, P. M.; Vogel, H. J. *Biochem. Cell Biol.* **1998**, *76*, 235–246.

(44) Brockman, H. *Curr. Opin. Struct. Biol.* **1999**, *9*, 438–443.

(45) Coccia, C.; Rinaldi, A. C.; Luca, V.; Barra, D.; Bozzi, A.; Di Giulio, A.; Veerman, E. C. I.; Mangoni, M. L. *Eur. Biophys. J.* **2011**, *40*, 577–588.

(46) Goraya, J.; Wang, Y.; Li, Z.; O'Flaherty, M.; Knoop, F. C.; Platz, J. E.; M, C. J. *Eur. J. Biochem.* **2000**, *267*, 894–900.

(47) Chinchar, V. G.; Wang, J.; Murti, G.; Carey, C.; Rollins-Smith, L. *Virology* **2001**, *288*, 351–357.

(48) Ogg, R.; Kingsley, P.; Taylor, J. *J. Magn. Reson. B* **1994**, *104*, 1–10.

(49) Smallcombe, S.; Patt, S. L.; Keifer, P. *J. Magn. Reson. A* **1995**, *117*, 295–303.

TABLES

Table 1. NMR Structure Quality and Calculation Statistics (standard deviation is reported in parenthesis).

	DPC	**DPC/SDS 3/1 mol/mol**
NMR restraints		
Short range NOEs[a]	20	20
Medium range NOEs[b]	7	26
Long range NOEs[c]	0	4
Total distance restraints from NOEs	27	50
Backbone dihedral angle restraints	28	30
Bonds statistics		
Average bond length deviation [Å]	0.002 (0.004)	0.01 (0.03)
Average bond angle deviation [deg]	0.34 (0.37)	1.25 (2.76)
Restraints violation statistics		
Average distance restraints violation [Å]	0.003 (0.019)	0.004 (0.015)
Maximum distance restraints violation [Å]	0.141[e]	0.094[f]
Average dihedral angle restraints violation [deg]	0.43 (1.29)	3.70 (6.43)
Maximum dihedral angle restraints violation [deg]	6.62[g]	20.73[h]
Structures root mean square deviation		
Backbone (global) [Å]	2.297 (0.810)	0.338 (0.120)
Backbone (folded segments)[d] [Å]	0.861 (0.343)	0.235 (0.122)

[a] Dipolar coupling between two residues i and j, where j=i+1.
[b] Dipolar coupling between two residues i and j, where $i+2 \leq j \leq i+4$.
[c] Dipolar coupling between two residues i and j, where $j \geq i+5$.
[d] DPC: residues 9 to 17; DPC/SDS: residues 2 to 7 and 9 to 17.
[e] Hβ(L6) – HN(A7).
[f] Hα(L15) – Hβ(S17).
[g] Ψ(K9).
[h] Φ(A7).

FIGURES

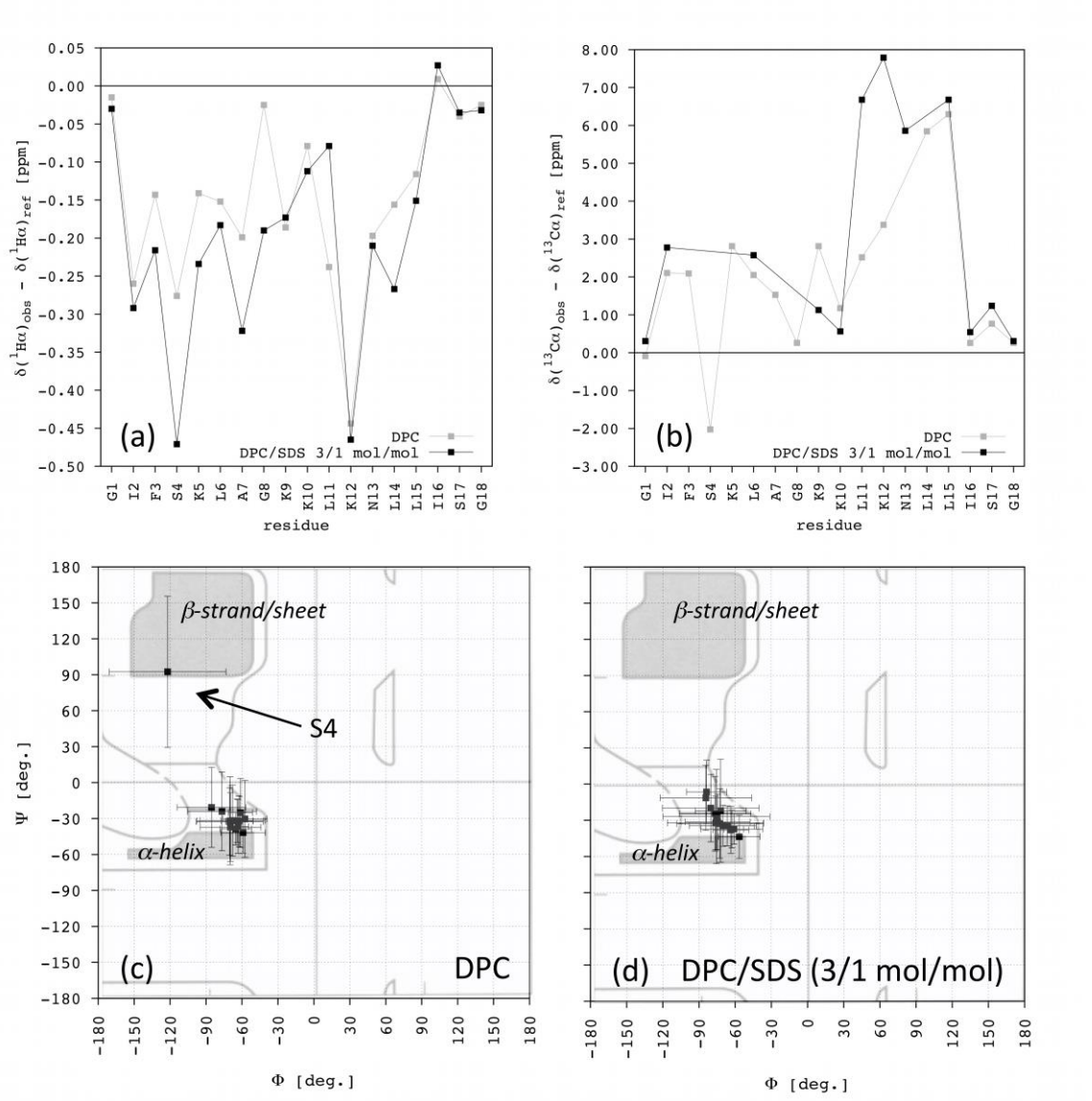

Figure 1. Deviation of the observed chemical shift from the reference 'random coil' values are reported for **(a)** ^{1}Hα and **(b)** ^{13}Cα. TALOS+ high-consensus predictions (residues from 2 to 7 and 9 to 16) are shown on the Ramachandran plot with the corresponding uncertainty. Results are shown for the case of either **(c)** DPC or **(d)** DPC/SDS 3/1 mol/mol micelles.

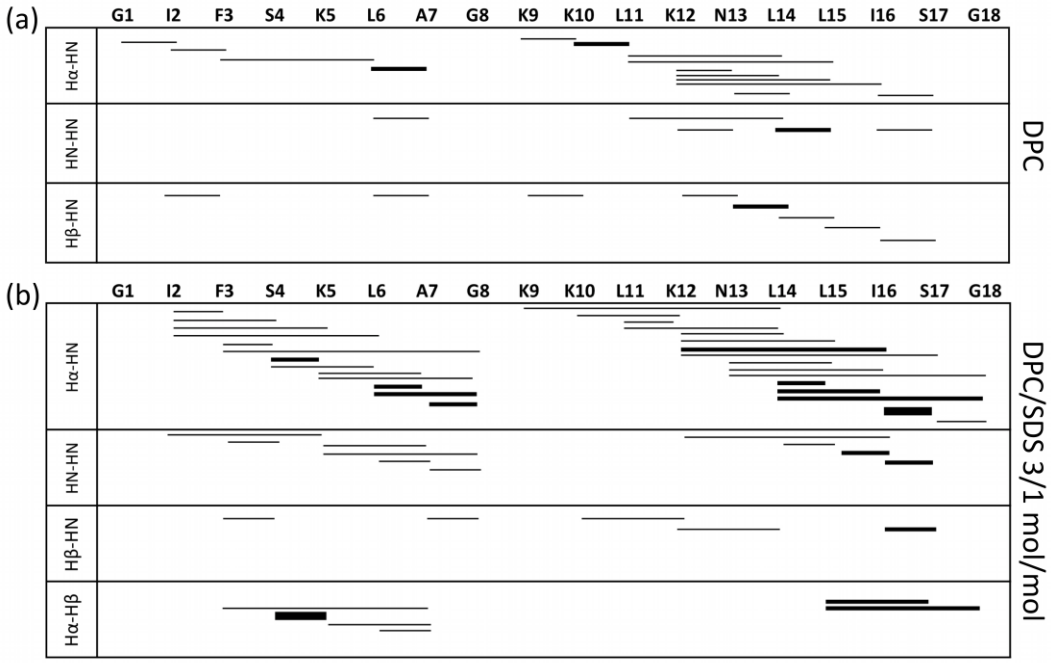

Figure 2. Interproton NOEs found for Esc(1-18) in the presence of **(a)** DPC and **(b)** DPC/SDS 3/1 mol/mol ratio. Correlations are reported as lines connecting the two residues involved. Line thickness is proportional to the relative intensity of the corresponding NOESY cross peak.

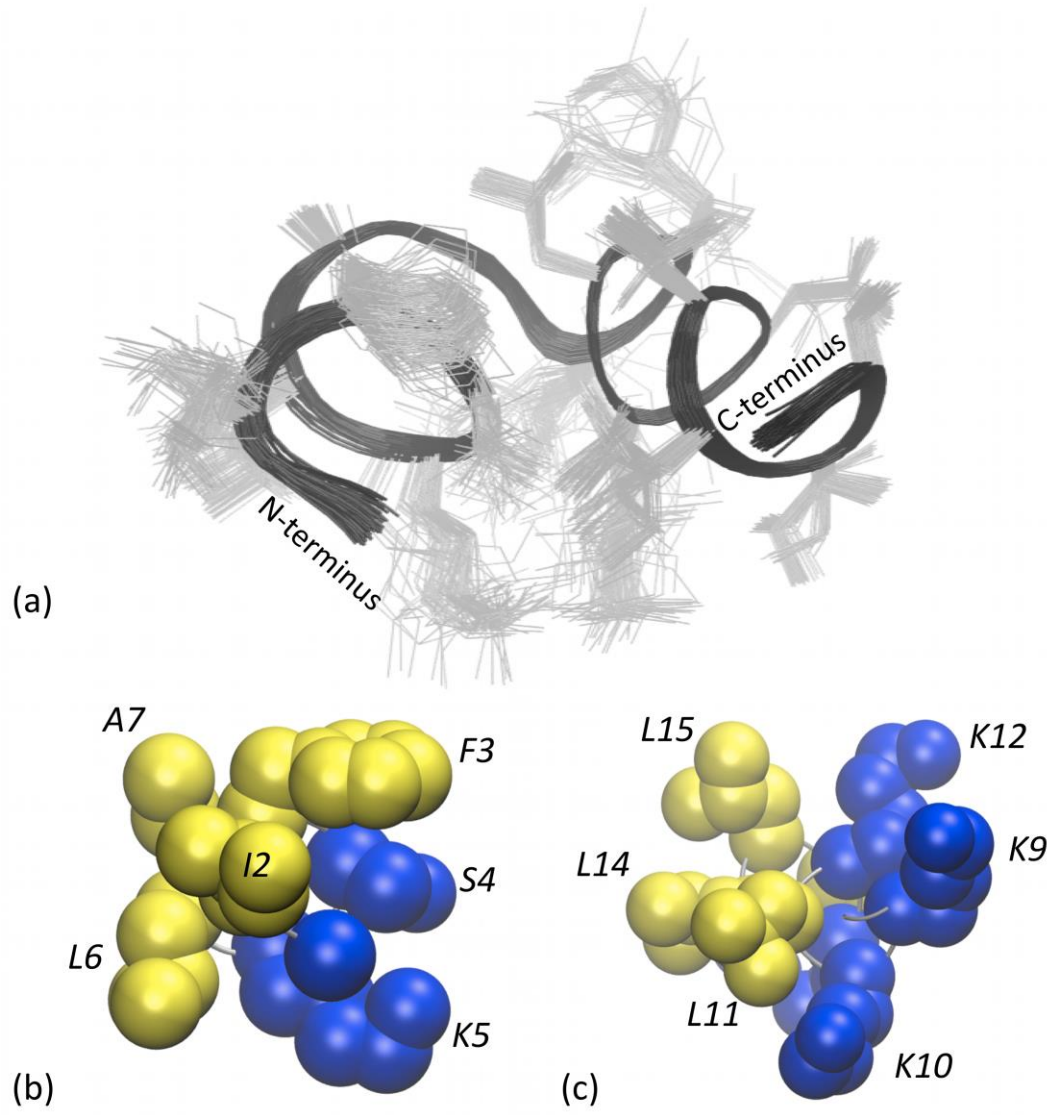

Figure 3. 3D structure of Esc(1-18) in DPC/SDS 3/1 mol/mol. **(a)** The backbone trace of the 100 structures with the lowest potential energy (black lines) together with sidechains (gray). The N-terminal **(b)** and the C-terminal helix **(c)** are shown for the conformer with the lowest RMSD from the average structure, with residues sidechains represented using atoms Van der Waals spheres and a different color, yellow and blue for the hydrophobic and the hydrophilic residues, respectively.

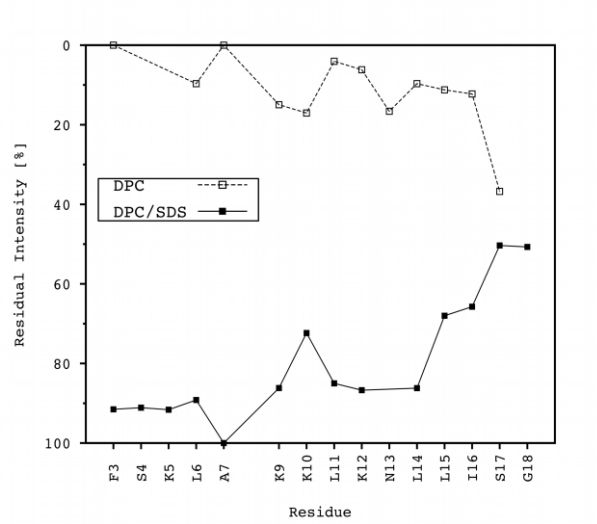

Figure 4. Results of the paramagnetic (Mn^{2+} 0.1 mM) relaxation enhancement experiments. Residual intensity of the NOESY cross-peaks in the HN-Hα region was calculated as the ratio between data acquired in the presence and absence of Mn^{2+}. The y-axis has been reversed in order to have solvent exposed residues at the top and protected residues at the bottom.

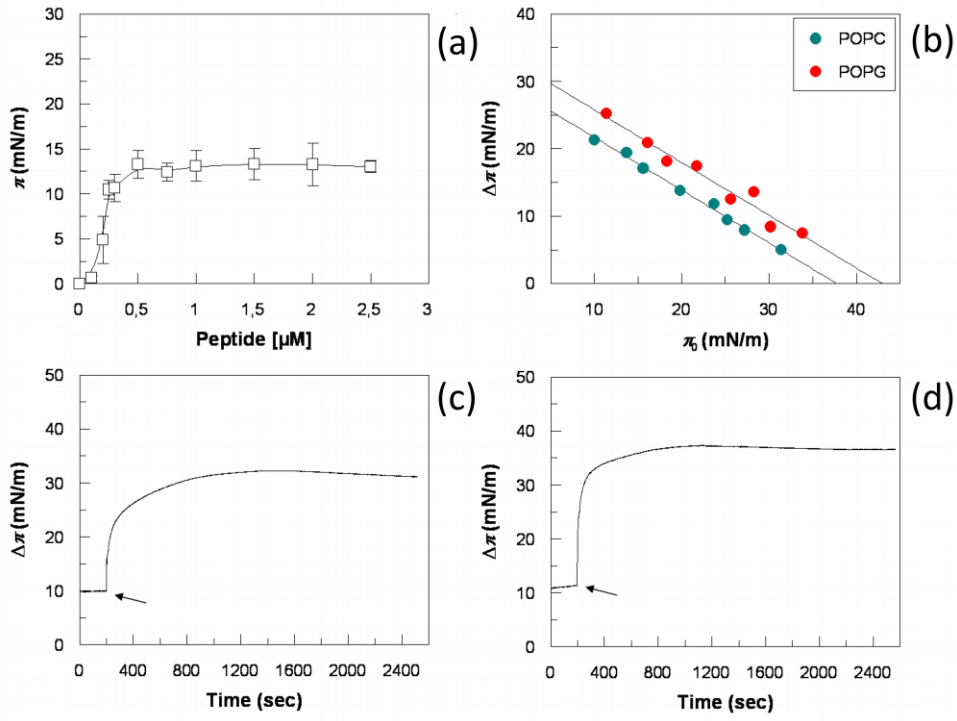

Figure 5. Insertion of Esc(1-18) into lipid monolayers. **(a)** The surface activity of Esc(1-18). The adsorption of peptide at the air/buffer (potassium phosphate 50 mM, pH 7, with 0.1 mM EDTA) interface was monitored as increasing surface pressure (π) over time. The maximum values of these surface pressures were plotted against peptide's final subphase concentration. Values are means ± SD of three independent measurements. **(b)** Increments of surface pressure of POPC and POPG monolayers due to the addition of 1.0 μM Esc(1-18) into the subphase are illustrated as a function of initial surface pressure (π_0). **(c)-(d)** Typical kinetics of surface pressure increase related to peptide's penetration into a POPC film (π_0 = 10.0) and into a POPG monolayer (π_0 = 11.3), respectively, are shown as representative of general trends. X-axis shows elapsed time (s). Peptide injection into the subphase took place at ≈ 200 s (arrow).

Table of Contents Graphics

SUPPORTING INFORMATION

The folded structure and insertion depth of the frog-skin antimicrobial peptide Esculentin-1b(1-18) in the presence of differently charged membrane mimicking micelles

G. Manzo,[†] M. Casu,[†] A. C. Rinaldi,[‡] N. P. Montaldo,[‡] A. Luganini,[§] G. Gribaudo,[§] M. A. Scorciapino[‡,]*

[†] Department of Chemical and Geological Sciences, University of Cagliari, Cittadella Universitaria, I-09042 Monserrato (CA), Italy

[‡] Department of Biomedical Sciences, University of Cagliari, Cittadella Universitaria, I-09042 Monserrato (CA), Italy[^]

[§] Department of Life Sciences and Systems Biology, University of Torino, I-10123 Torino, Italy

* to whom correspondence should be addressed:

Dr. **Mariano Andrea Scorciapino**, Ph.D.

Department of Biomedical Sciences

University of Cagliari

Cittadella Universitaria

I-09042 Monserrato (CA)

Italy

tel: +39-070-675-3921

fax: +39-070-675- 4527

e-mail: scorciapino@unica.it

Table S1. ^{1}H and ^{13}C resonance assignments for Esc(1-18) in the presence of either DPC or DPC/SDS 3/1 mol/mol micelles (phosphate buffer solution 10 mM, pH 7.4).

	DPC						DPC/SDS 3/1 mol/mol					
	^{1}H (ppm)				^{13}C (ppm)		^{1}H (ppm)				^{13}C (ppm)	
Residue	**H_N**	**Hα**	**Hβ**	**Others**	**Cα**	**Cβ**	**H_N**	**Hα**	**Hβ**	**Others**	**Cα**	**Cβ**
G1	---	3.966 3.924			45.010		---	3.930			45.405	
I2	8.347	3.910	1.780	1.388 γ_1' 1.162 γ_1'' 0.725 γ_2 0.836 δ_1	63.405	37.972	8.315	3.878	1.765	1.417 γ_1' 1.165 γ_1'' 0.705 γ_2 0.854 δ_1	64.077	38.251
F3	8.659	4.384	3.202 3.145	7.262 δ 7.220 ε 7.126 ζ	60.090	38.049	8.382	4.311	3.232 3.152	7.279 δ 7.162 ε 7.060 ζ	---	---
S4	8.361	4.194	4.029 3.964		56.176	62.685	8.522	3.999	---		---	---
K5	7.795	4.179	1.904	1.569 γ 1.702 δ 2.947 ε	59.099	32.131	7.920	4.086	1.966	1.452 γ 1.666 δ 2.972 ε	---	32.339
L6	7.862	4.188	1.790 1.586	--- γ 0.946 δ_1 0.881 δ_2	56.889	42.151	8.016	4.157	1.979	1.875 γ 0.892 $\delta_{1,2}$	57.413	---
A7	7.952	4.121	1.335		53.565	18.570	8.369	3.998	1.307		---	18.476
G8	a	a			a		8.482	---			---	
K9	8.061	4.134	1.898	1.498 γ 1.697 δ 2.982 ε	59.099	32.131	7.944	4.147	1.883	1.594 γ 1.719 δ 2.991 ε	57.413	32.339
K10	8.064	4.241	1.923	1.505 γ 1.736 δ 2.948 ε	59.099	32.131	7.838	4.208	1.853	1.561 γ 1.821 δ 2.916 ε	56.851	32.339
L11	8.286	4.102	1.780 1.659	1.750 γ 0.937 δ_1 0.895 δ_2	57.357	41.469	7.962	4.261	1.952	1.801 γ 0.900 $\delta_{1,2}$	61.520	---
K12	8.278	3.876	1.897	1.454 γ 1.707 δ 2.917 ε	59.664	32.131	8.313	3.855	1.944	1.497 γ' 1.460 γ'' 1.732 δ 2.925 ε	64.077	32.339
N13	7.935	4.543	2.887	--- δ	---	---	---	4.530	2.920	7.738 δ' 6.932 δ''	53.139	---
L14	7.862	4.184	1.886 1.685	1.804 γ 0.946 δ_1 0.880 δ_2	60.686	42.200	8.424	4.073	1.842	1.820 γ 0.953 $\delta_{1,2}$	---	---
L15	7.770	4.224	1.819 1.614	1.802 γ 0.914 δ_1 0.875 δ_2	61.134	42.151	7.995	4.189	1.932	1.875 γ 0.915 $\delta_{1,2}$	61.520	---
I16	7.794	4.179	2.013	1.554 γ_1' 1.280 γ_1'' 0.942 γ_2 0.881 δ_1	61.557	38.256	7.877	4.197	2.052	1.572 γ_1' 1.320 γ_1'' 0.957 γ_2 0.887 δ_1	61.841	38.441
S17	8.172	4.430	3.967		58.967	63.609	8.136	4.435	3.974		59.437	63.958
G18	a	a			a		8.314	3.928			45.405	

[a] The resonances from G8 and G18 were not unambiguously identified in the presence of pure DPC micelles.

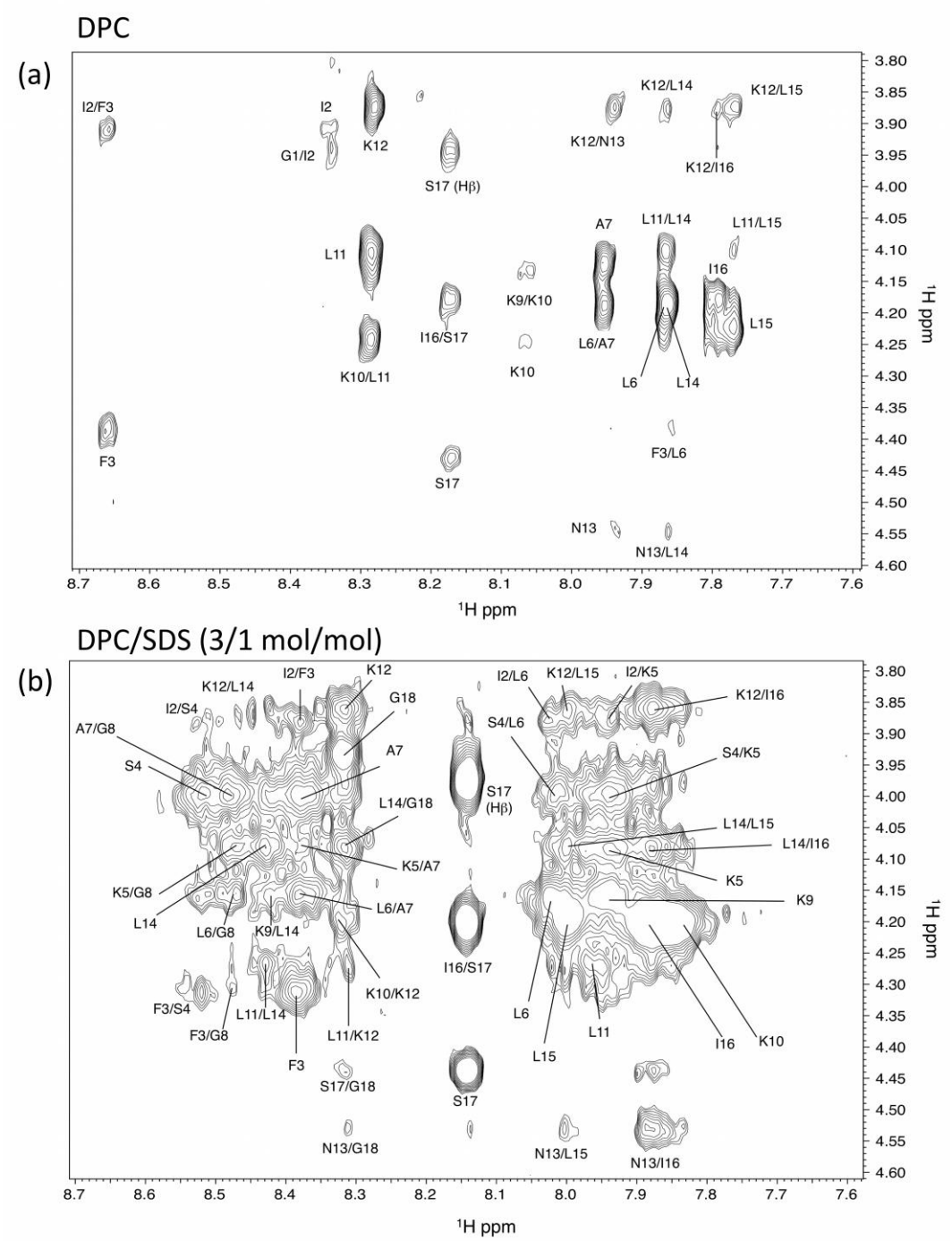

Figure S1. The Hα-HN region of the NOESY spectra of Esc(1-18) acquired in the presence of **(a)** DPC and **(b)** DPS/SDS micelles.

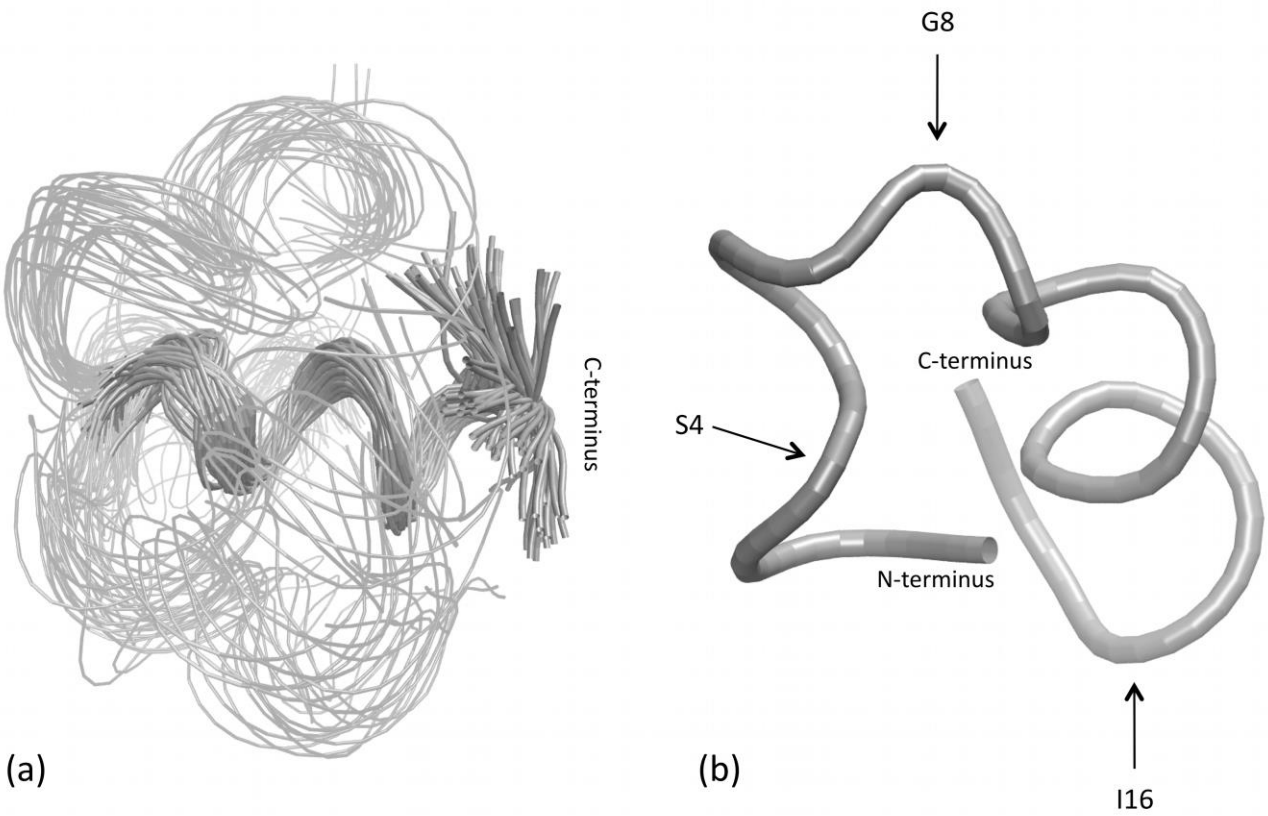

Figure S2. Backbone trace of Esc(1-18) in the presence of DPC micelles. **(a)** The 100 conformers with the lowest potential energy are superimposed after alignment of the C-terminal helical segment. This specific alignment was chosen for graphical reasons: the poor resolution of the N-terminal segment would result in a bad global structure alignment and, in turn, an image lacking any informative content. Here, the N-terminal segment is represented with a lower thickness than the C-terminal one, in order to make the latter visible. **(b)** The conformer with the lowest RMSD from the average structure is shown together with labels indicating the position of selected residues.

RESULTS AND DISCUSSION OF ANTIVIRAL ACTIVITY

Esc(1-18) does not exert an antiviral activity against Herpes simplex virus type 1 (HSV-1). In a previous study, it has been reported that esculentin-2P (Esc-2P) isolated from *Rana pipiens*[1] decreased infectivity of the Channel Catfish Virus (CCV), a herpesvirus that infects cold-blooded animals, by interacting with and disrupting the virus lipid bilayer envelope and therefore inhibiting the infection.[2] Since lipid membrane perturbation has been also suggested as the main mechanism of action of Esc(1-18) against both bacteria[3] and yeasts,[4] we investigated further the Esc(1-18) biological activities by evaluating its effects on the infectivity and replication of HSV-1, a prototype of large DNA viruses endowed with a lipid bilayer envelope required for infectivity.[5] To investigate a direct effect of Esc(1-18) on HSV-1 infectivity, aliquots of virus particles were incubated with various concentrations of Esc(1-18) either at 4 or 37 °C for 2 hours. After incubation, samples were titrated for residual infectivity on Vero cells. As shown in Figure S3a, in the presence of Esc(1-18) there was no significant loss of infectivity both at 4 °C and 37 °C, since virus titers of samples exposed to Esc(1-18) were comparable to that determined in the untreated sample. Yet, we observed in every sample (also for the untreated ones) an about 1 Log reduction in virus infectivity after incubation at 37 °C. However, this reduction might be ascribed to the effect of temperature on virus infectivity. Ascertained that Esc(1-18) is not able to inhibit viral infectivity, we investigated whether a pretreatment with the peptide could affect HSV-1 replication in infected cells. In these virus yield reduction assays, Esc(1-18) was present in cell medium before, during, and after viral adsorption. As shown in Figure S3b, pretreatment of cells prior virus addition and treatment with Esc(1-18) had only a minimal effect of HSV-1 replication (about 30% reduction in viral yield) at the maximum concentration tested in the assay (80 μM). Moreover, Esc(1-18) did not significantly affect the viability of Vero cells, as >90% of cells were still viable after 3 days of treatment with concentrations as high as 80 μM, thus suggesting that the minimal antiviral activity of the peptide at this concentration cannot be ascribed to non-specific cytoxicity of the target cells themselves (Figure S3b). In conclusion, Esc(1-18), despite its antibacterial and antifungal activities,

seems to be devoid of a direct virucidal activity against herpeviruses, while it has been reported for Esc-2P against CCV.[1] It is not known whether this reflects differences in the peptides or in the target viruses. Esc-2P, for which no detailed structural characterization nor membrane-affinity study is currently available, is characterized by the presence of a seven-membered C-terminal disulphide ring (GFSSIFRGVAKFASKGLGKDLARLGVNLVACKISKQC) and share little sequence homology with Esc(1-18). Thus, it is likely that differences in the amino acid sequence of the two peptides may account for the lack of a significant antiviral activity of Esc(1-18) against herpesviruses. Further studies with different enveloped and noneveloped viruses will be required to assess the efficacy, if any, of Esc(-18) against viral pathogens.

EXPERIMENTAL SECTION

Antiviral Assays. African green monkey kidney cells (Vero) (ATCC CCL-81) were cultured in Eagle's minimal essential medium (MEM; Gibco-BRL) supplemented with 10% fetal bovine serum (FBS; Gibco-BRL), 1 mM sodium pyruvate, 2 mM glutamine, 100 U/ml penicillin, and 100 μg/ml streptomycin sulfate. A clinical isolate of Herpes simplex type 1 virus (HSV-1) sensitive to acyclovir, kindly provided by V. Ghisetti (Amedeo di Savoia Hospital, Turin), was propagated and titrated by standard plaque assay on Vero cells as described previously.[6]

To assess the direct effect of Esc(1-18) on HSV-1 infectivity, a procedure based on that of Shogan et al.[7] was followed, with minor modifications as described by Luganini et al.[6] To this end, various concentrations of Esc(1-18) were added to aliquots of HSV-1 (10^5 PFU), and the virus-peptide samples were incubated at either 4 or 37 °C for 2 h, and then their residual infectivity was titrated on Vero cells. A viral inoculum, treated with medium without the peptide, was used as a control. Plaques were microscopically counted, and the mean plaque counts for each peptide concentration were expressed as PFU/ml on a log10 scale.

The effect of Esc(1-18) on HSV-1 replication was evaluated by a virus yield reduction assay.[6] Briefly, Vero cells were treated with serial dilutions of Esc(1-18) for 2 hours at 37 °C before

infection with HSV-1 at an MOI of 0.1. Following virus adsorption (2 h at 37 °C), the cultures were maintained in medium containing the corresponding concentration of peptide and then incubated for 48 h post infection (p.i.) until the control sample displayed extensive cytopathology. Hence, the cells and supernatants were pooled, and the extent of virus replication was assessed by standard plaque assay on Vero cells. Plaques were expressed as a percentage of the mean plaque count of the control virus and the value obtained was plotted as function of drug concentration to determine the concentration producing 50% (IC50) reduction in plaque formation. To determine cell viability, Vero cells were exposed to increasing concentrations of peptides. After 3 days of incubation, the number of viable cells was determined using the 3-(4,5-dimethylthiazol-2-yl)-2,5-diphenyltetrazolium bromide (MTT) method, as previously described.[8]

REFERENCES

(1) Goraya, J.; Wang, Y.; Li, Z.; O'Flaherty, M.; Knoop, F. C.; Platz, J. E.; M, C. J. *Eur. J. Biochem.* **2000**, *267*, 894–900.

(2) Chinchar, V. G.; Wang, J.; Murti, G.; Carey, C.; Rollins-Smith, L. *Virology* **2001**, *288*, 351–357.

(3) Marcellini, L.; Borro, M.; Gentile, G.; Rinaldi, A. C.; Stella, L.; Aimola, P.; Barra, D.; Mangoni, M. L. *FEBS J.* **2009**, *276*, 5647–5664.

(4) Luca, V.; Olivi, M.; Di Grazia, A.; Palleschi, C.; Uccelletti, D.; Mangoni, M. L. *Cell. Mol. Life Sci.* **2013**.

(5) Roizman, B.; Knipe, D. M.; Whitley, R. J. In *Fields Virology - vol.2*; Knipe, D. M.; Howley, P. M., Eds.; Lippincott, Williams & Wilkins: Philadelphia, 2013; pp. 1823–1897.

(6) Luganini, A.; Nicoletto, S. F.; Pizzuto, L.; Pirri, G.; Giuliani, A.; Landolfo, S.; Gribaudo, G. *Antimicrob. Agents Chemother.* **2011**, *55*, 3231–3239.

(7) Shogan, B.; Kruse, L.; Mulamba, G. B.; Hu, A.; Coen, D. M. *J. Virol.* **2006**, *80*, 4740–4747.

(8) Pauwels, R.; Balzarini, J.; Baba, M.; Snoeck, R.; Schols, D.; Herdewijn, P.; Desmyter, J.; De Clercq, E. *J. Virol. Methods* **1988**, *20*, 309–321.

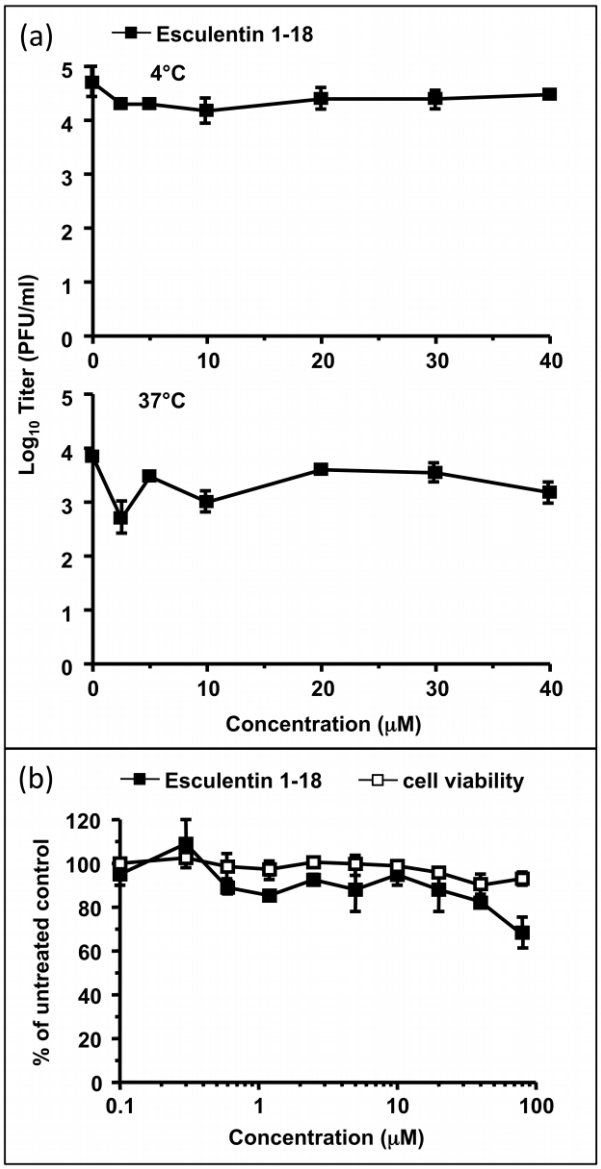

Figure S3. Effect of Esc(1-18) on HSV-1 infectivity and replication. **(a)** Esc(1-18) does not exert a direct virucidal effect on HSV-1. HSV-1 aliquots (10^5 PFU) were incubated at either 4 or 37 °C for 2 h with different concentrations of Esc(1-18). Then, the viral infectivity was evaluated titrating the peptide-virus samples by plaque assay. The data shown represent means ± SD (error bars) of three independent experiments performed in duplicate. **(b)** Esc(1-18) does not influence significantly HSV-1 replication in infected cells. Vero cells were infected at a MOI of 0.1 pfu/cell and, where indicated, the cells were pretreated and treated with increasing concentrations of Esc(1-18) 2 h prior, as well as during virus adsorption and throughout the experiment until an extensive viral cytopathic effect was observed in the untreated control. The extent of viral replication was then assessed by titrating the infectivity of supernatants of cells suspensions using a standard plaque assay. Plaques were microscopically counted and the mean plaque counts for each drug concentration expressed as a percentage of the control mean count. Data shown represent means ± SD (error bars) of three independent experiments performed in duplicate.